Determination of the Rate Coefficient for the Reaction H + O_2 → OH + O by a Shock Tube/Laser Absorption/Detailed Modeling Study

T. Yuan, C. Wang, C.-L. Yu, M. Frenklach,*

Fuel Science Program, Department of Materials Science and Engineering, The Pennsylvania State University, University Park, Pennsylvania 16802

and M. J. Rabinowitz

NASA-Lewis Research Center, Cleveland, Ohio 44135 *(Received: June 4, 1990; In Final Form: August 17, 1990)*

Mixtures of hydrogen and oxygen diluted in argon were studied behind reflected shock waves at temperatures from 1050 to 2700 K. The reaction progress was measured in situ by state-selective laser absorption of OH radicals. Solution mapping methodology was employed to interpret the experimental results, quantifying the effects of all active rate parameters. The rate coefficient expression for the key reaction in the system, H + O_2 → OH + O, derived was $k_1 = 1.59 \times 10^{17} T^{-0.927} e^{-8493/T}$ cm^3 mol^{-1} s^{-1} with one standard deviation of 0.05 for log k_1. The analysis indicates that under no physically realistic conditions could the values of k_1 reach those reported by Frank and Just (1985), and that in most cases the k_1 temperature-dependent expression is close to the results of Schott (1973).

Introduction

The title reaction

$$H + O_2 \rightarrow OH + O \qquad (R1)$$

plays the key role in high-temperature combustion of fossil fuels—it governs the chain branching in the main reaction zone of hydrocarbon flames.[1,2] Practically all flame properties exhibit their largest sensitivity to the rate coefficient of this reaction, k_1.[1,3] For instance, a 10% change in the value of k_1 alters the computed flame speed of a stoichiometric methane–air laminar premixed flame by about 2 cm/s out of the nominal speed of 40 cm/s. Not only is accuracy in k_1 important for practical applications of flame modeling, but it also affects identification of kinetic parameters of other reactions, e.g., those responsible for the formation of NO_x[4] and soot,[5] in combustion-chemistry experiments. Therefore, k_1 must be known with extreme accuracy for successful progress in combustion modeling.

The rate coefficient k_1 has been measured[6-12] and reviewed[1,13-15] by several investigators (a detailed review of the literature is given in ref 16). However, the values determined and recommended in these studies span about a factor of 2 at high temperatures, which is an unacceptable level of uncertainty for such a critical parameter. Here we report the results of a new experimental and modeling study using a series of H_2–O_2–Ar shock-heated mixtures, in which OH concentration was monitored in situ by a quantitative laser absorption technique. The k_1 temperature expression was determined by extensive computer modeling with particular emphasis on analysis and quantification of systematic errors.

Experimental Section

Shock Tube Apparatus. The experiments were performed in a conventional shock tube, made of a constant-diameter stainless-steel tube with an internal diameter of 7.94 cm and a wall thickness of 3.2 mm. The end plate of the shock tube was made of aluminum. The driver and driven sections were 1.5 and 4.9 m long, respectively. A double-diaphragm burst technique was used to initiate the shock waves. The diaphragms were made of Mylar film. Prior to each experiment, the driven section of the shock tube was evacuated to at least 1×10^{-5} Torr by an oil diffusion pump equipped with water- and liquid-nitrogen-cooled traps. The shock tube was tested for leaks by a Varian PortaTest leak detector and was cleaned after every experimental run. The possible interference of the molecular desorption from the shock tube walls, contributing to the chain branching, was tested by blank runs with a 1% O_2–Ar mixture—no OH absorption signal was detected below 2600 K. Above this temperature, a slight absorption was observed, equivalent to OH concentration computed with about 10–15 ppm of H_2 present in the mixture.

The test mixtures were prepared manometrically, with the maximum uncertainty in the final reactant concentrations of about 3%, and allowed to mix in a stainless steel tank for 24 h prior to experimental runs. The stated purity of gases used in preparation of these mixtures were H_2 99.9999%, O_2 99.999%, and Ar 99.9999%. The driver gas was helium 99.998%. All the gases were used as purchased, without further purification.

The postshock conditions were calculated from the incident shock velocity in the usual manner,[17] assuming no chemical reaction and full vibrational relaxation. The thermodynamic data compiled by Burcat was used in these calculations.[18] The incident shock velocity was determined by four PCB Model 482A piezoelectric pressure transducers mounted 25.4 cm apart, the last one being located 12.7 mm from the end plate. All pressure transducers and optical windows were mounted flush with the

(1) Warnatz, J. In *Combustion Chemistry*; Gardiner, W. C., Jr., Ed.; Springer-Verlag: New York, 1984; p 197.
(2) Westbrook, C. K.; Dryer, F. D. *Prog. Energy Combust. Sci.* **1984**, *10*, 1.
(3) Nowak, U.; Warnatz, J. *Prog. Astronaut. Aeronaut.* **1988**, *113 I*, 87.
(4) Miller, J. A.; Bowman, C. T. *Prog. Energy Combust. Sci.* **1989**, *15*, 287.
(5) Frenklach, M.; Wang, H. *Symp. (Int.) Combust., [Proc.] 23*, to be published.
(6) Schott, G. L. *Combust Flame* **1973**, *21*, 357.
(7) Chiang, C. C.; Skinner, G. B. In *Shock Tubes and Waves*; Lifshitz, A., Rom, J., Eds.; Magnes: Jerusalem, Israel, 1980; p 629.
(8) Dixon-Lewis, G. *Combust. Sci. Technol.* **1983**, *34*, 1.
(9) Frank, P.; Just, Th. *Ber. Bunsen-Ges. Phys. Chem.* **1985**, *89*, 181.
(10) Fujii, N.; Shin, K. S. *Chem. Phys. Lett.* **1988**, *151*, 461.
(11) Pirraglia, A. N.; Michael, J. V.; Sutherland, J. W.; Klemm, R. B. *J. Phys. Chem.* **1989**, *93*, 282.
(12) Koike, T. *Bull. Chem. Soc. Jpn.* **1989**, *62*, 2480.
(13) Baulch, D. L.; Drysdale, D. D.; Horne, D. G.; Lloyd, A. C. *Evaluated Kinetic Data for High Temperature Reactions*; Butterworths: London, 1972; Vol. 1.
(14) Cohen, N.; Westberg, K. R. *J. Phys. Chem. Ref. Data* **1983**, *12*, 531.
(15) Dixon-Lewis, G. In *Complex Chemical Reaction Systems, Mathematical Modelling and Simulation*; Warnatz, J., Jäger, W., Eds.; Springer-Verlag: Berlin, 1987; p 265.
(16) Yuan, T.-F. Soot Formation in Pyrolysis and Oxidation of Hydrocarbons. Ph.D. Thesis, Department of Materials Science and Engineering. The Pennsylvania State University, 1990.
(17) Gardiner, W. C., Jr.; Walker, B. F.; Wakefield, C. B. In *Shock Waves in Chemistry*; Lifshitz, A., Ed.; Dekker: New York, 1981; p 319.
(18) Burcat, A. In *Combustion Chemistry*; Gardiner, W. C., Jr., Ed.; Springer-Verlag: New York, 1984; p 455.

0022-3654/91/2095-1258$02.50/0

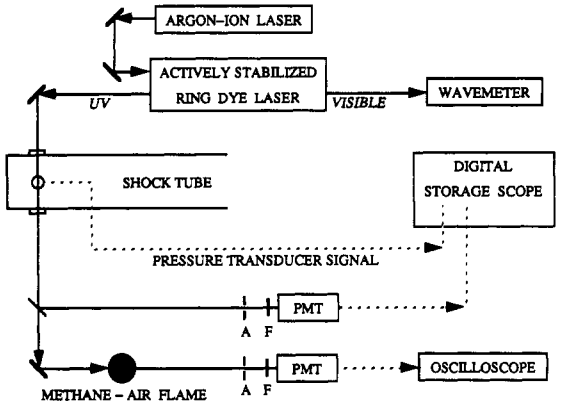

Figure 1. Schematic diagram of the optical detection system.

inside surface of the shock tube to minimize the distortion to the gas flow. The velocity of the incident shock was extrapolated to the end plate,[19] and this extrapolated velocity was then used in the calculations of the temperature, T_5, pressure, P_5, and total density, C_5, of the gas behind the reflected shock waves. The observed shock wave attenuation was less than 1.5%/m. The maximum uncertainty in the time measurements was estimated to be ±0.5 μs, which corresponded to ±0.35% and ±0.09% uncertainties in the computed values of T_5 and C_5, respectively.

Optical Detection System. The progress of reaction was monitored by measuring the concentration of the OH radical using state-selective absorption spectroscopy developed by Hanson and co-workers.[20] A schematic diagram of the optical detection system is shown in Figure 1. An actively stabilized Coherent CR-699-21 ring-dye laser was pumped by a Coherent Innova 100-15 argon ion laser. The resulting beam was frequency-doubled and carefully tuned to the center of the OH spectral $P_1(5)$ line, (0,0) band of the $A^2\Sigma^+$–$X^2\Pi$ transition (310.123 nm). The argon ion laser was operated under single-line output (514.5 nm) and current regulation modes to assure a constant temperature in the laser cavity so that a constant output beam path could be maintained. A Coherent Model 7500 frequency doubler ($LiIO_3$ crystal) and a Coherent etalon assembly (ICA) were installed in the cavity of the ring-dye laser. Kiton-red dye was used in this work. The dye solution was circulated by a Coherent 5920 Dye Circulator with pressure maintained at 40 psi. The dye solution was cooled by water as well as a Neslab CFT-25 Refrigerated Recirculator to maintain a constant temperature of 10 °C in order to achieve maximum conversion efficiency. The wavelength of the primary laser beam (620.246 nm) was monitored by a Burleigh WA-10 wavemeter, which has an accuracy of ±0.001 nm.

The generated single-frequency secondary beam, centered at 310.123 nm with a line width of 2 MHz and typically at a 3-mW power level, passed through the center of the shock tube, 12.7 mm away from the end plate (Figure 1). Shock tube windows were made of quartz. The wavelength of the secondary beam was fine-tuned to the center of the absorption line by passing the beam through the center of a methane flame, the procedure suggested by Hanson et al.[20] The intensity of the transmitted (secondary) beam was measured by a THORN EMI 9924B photomultiplier tube (PMT), which has a specified rise time of 15 ns. A narrow-band interference filter was mounted on the PMT to minimize the background emission from the shocked gases. The lasers and the optical instruments were set on an air-floated NRC KL-A optical table to reduce vibrational disturbances. The PMT signal, along with the signal generated by the pressure transducer located at the observation section, were recorded by a Nicolet 2070 dual-channel digital oscilloscope. The overall time constant of the light detection system, τ, was 0.6 μs, as determined by using a strobe light source.

Time Constant Correction. This time constant was built into the kinetic code in the following manner.[21] The system of differential equations describing the time evolution of the reaction system was augmented with the differential equation

$$\frac{dA'}{dt} = \frac{1}{\tau}(A - A') \tag{1}$$

where t is the reaction time, A is the actual absorbance ($A = (I_0 - I)/I_0$, where I_0 and I are the incident and transmitted light intensities or the corresponding photomultiplier output electric currents, respectively) and A' is the transformed absorbance, i.e., the signal transformed by the electronic circuit with a time constant τ ($A' = (U_0 - U)/U_0$, where U_0 and U are the voltages, corresponding to I_0 and I on the entrance to the oscilloscope). Assuming the Beer–Lambert law, $I/I_0 = e^{-\epsilon l[OH]}$, eq 1 takes the form

$$\frac{d[OH]'}{dt} = \frac{1}{\epsilon l \tau}(1 - e^{-\epsilon l([OH]-[OH]')}) \tag{2}$$

where ϵ is the absorption coefficient, l is the optical path, [OH] is the actual OH concentration (as computed by the kinetic mechanism), and [OH]′ is the transformed concentration, i.e., the signal transformed by the electronic circuit with a time constant τ. At small absorbance values, i.e., when $\epsilon l\{[OH] - [OH]'\} \ll 1$, eq 2 is well approximated by

$$\frac{d[OH]'}{dt} = \frac{1}{\tau}([OH] - [OH]') \tag{3}$$

OH concentration computed in this manner was compared with the experimental counterpart.

Absorption Coefficient. The OH absorption coefficient was calculated theoretically, following the recent recommendations of Larsson[22]

$$\epsilon_{\nu_0} = \frac{\pi e^2}{m_e c^2}\frac{n''}{n} f_{lu}(1 - e^{-h\nu_0/k_B T}) g(\nu_0) \tag{4}$$

where ϵ_{ν_0} is the absorption cross section at the center-line transition frequency ν_0, e and m_e are the charge and mass of electron, c is the speed of light, n is the total number density of OH, n'' is the number density of OH in the lower state, $g(\nu_0)$ is the value of the Voigt profile at the line center, T is temperature, k_B and h are the Boltzmann and Planck constants, respectively, and f_{lu} is the line absorption oscillator strength. The latter was calculated as[22-24]

$$f_{lu} = \frac{f_{\nu'\nu''} S_{J'J''} T_{J'J''}}{2J'' + 1}$$

where $f_{\nu'\nu''}$ is the $\nu' \leftarrow \nu''$ band absorption oscillator strength, $S_{J'J''}$ is the $J' \leftarrow J''$ rotational line intensity (Hönl–London) factor, and $T_{J'J''}$ is the correction factor due to the vibration–rotation interaction. For the P1(5) line of the (0,0) band employed in our study, $f_{\nu'\nu''} = 1.1 \times 10^{-3}$ (ref 25), $S_{J'J''} = 6.13$ [ref 26 for Hund's case b], $T_{J'J''} = 0.978$ (ref 27), thus giving $f_{lu} = 5.5 \times 10^{-4}$. The value of n'' was calculated from the Boltzmann equation with the assumption of local thermal equilibrium[28]

$$n'' = \frac{n(2J'' + 1)e^{-(E_1+E_2)/k_B T}}{Q}$$

(19) Bornside, D. E. Ignition in Methane-Additive Mixtures. M.S. Thesis, Department of Chemical Engineering, Louisiana State University, 1983.
(20) Hanson, R. K.; Salimian, S.; Kychakoff, G.; Booman, R. A. *Appl. Opt.* **1983**, *22*, 641.
(21) Frenklach, M. Study of the Kinetics of High Temperature Gas Phase Reactions by Shock Wave Technique. Ph.D. Thesis, Department of Physical Chemistry, Hebrew University, Jerusalem, Israel, 1976.
(22) Larsson, M. *Atron. Astrophys.* **1983**, *128*, 291.
(23) Whiting, E. E.; Schadee, A.; Tatum, J. B.; Hougen, J. T.; Nicholls, R. W. *J. Mol. Spectrosc.* **1980**, *80*, 249.
(24) Schadee, A. *J. Quant. Spectrosc. Radiat. Transfer* **1979**, *19*, 451.
(25) Smith, G. P.; Crosley, D. R. *Symp. (Int.) Combust. [Proc.]* **1981**, *18*, 1513.
(26) Goldman, A.; Gillis, J. R. *J. Quant. Spectrosc. Radiat. Transfer* **1981**, *25*, 111.
(27) Crosley, D. R.; Lengel, R. K. *J. Quant. Spectrosc. Radiat. Transfer* **1975**, *15*, 579.

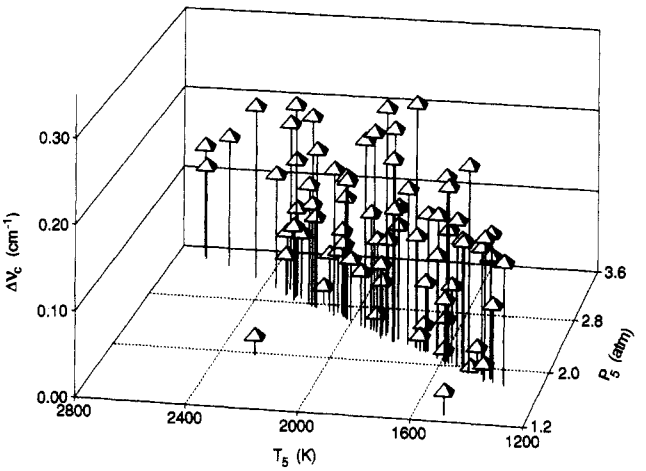

Figure 2. Collision broadening as a function of temperature and pressure.

where E_v and E_J are the vibrational and rotational energies, respectively, and Q is the total partition function. E_v and E_J were calculated by using the vibrating–rotator model.[29] The partition function Q was calculated by using a higher order approximation of the thermodynamic functions for a diatomic molecule.[30] The center-line Voigt profile value was calculated as[31,32]

$$g(\nu_0) = \frac{1}{\Delta\nu_D}\left[\frac{\ln 2}{\pi}\right]^{1/2} e^{a^2}\left(1 - \frac{2}{\pi^{1/2}}\int_0^a e^{-u^2}\,du\right) \qquad (5)$$

where

$$a = \frac{\Delta\nu_c}{\Delta\nu_D}(\ln 2)^{1/2}$$

$$\Delta\nu_D = \nu_0\left[\frac{2 \ln 2\, k_B T}{m_c c^2}\right]^{1/2}$$

and $\Delta\nu_c$ is the collision broadening half-width.

The principal difficulty in calculating the absorption coefficient by eq 4 is the lack of fundamental knowledge on the collision-broadening parameter, $\Delta\nu_c$ in eq 5. It has been suggested[31,33] to resolve this empirically: to express $\Delta\nu_c$ in the form

$$\Delta\nu_c = \gamma P\left(\frac{T_{ref}}{T}\right)^n \qquad (6)$$

and to determine free parameters γ and n from experiment; here P and T are the system pressure and temperature, respectively, and T_{ref} is the reference temperature. In an attempt of adopting this strategy, we determined the values of $\Delta\nu_c$ by fitting the maximum in the absorption signal for each individual experiment; it was established by a sensitivity analysis, which will be discussed below, that the maximum OH concentration does not show significant sensitivity to rate parameters under the conditions of the present study. Figure 2 depicts the obtained values of $\Delta\nu_c$ plotted against experimental pressure and temperature. Although the range of $\Delta\nu_c$ is found to be in good agreement with the results of Rea et al.,[33] no systematic trend with pressure or temperature can be clearly observed in Figure 2. More importantly, the level of scatter in individual determinations of $\Delta\nu_c$ is relatively high—unacceptable for the objectives of the present work. Based on these considerations, we choose an alternative way of analyzing the experimental results.

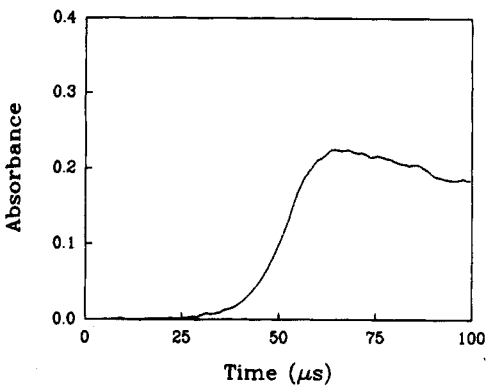

Figure 3. A typical OH absorption profile, obtained in a 2.0% H_2–0.5% O_2–Ar mixture at T_5 = 1914 K and P_5 = 2.47 atm.

Experimental Conditions

Absorption profiles obtained under the conditions used in the present study all appeared as in Figure 3: after an induction period, the absorption rapidly increases, reaches a maximum (corresponding to the maximum of OH concentration), and then slowly declines. It was established by sensitivity analysis that the maximum absorption, as well as the rest of the profile after the maximum, does not show significant sensitivity to rate coefficients of the H_2–O_2 system. Since the a priori determination of the absorption coefficient was unreliable, as discussed in the previous section, it was calculated for every experiment by fitting the corresponding maximum OH absorption, and the kinetic information was then extracted by matching the initial part of the absorption profile.

Six series of experiments with different initial mixture compositions were used in the course of this study; their experimental conditions are summarized in Table I. Selection of the mixtures was based on the following considerations:

1. The sensitivity of the initial OH profile to k_1. It was noticed in a preliminary sensitivity analysis that variations in the rate coefficients have little effect upon the shape of the initial part of the OH absorption profile, but merely shift the profile along the time axis. Therefore, the ranking sensitivities of the OH profile with respect to the rate constants were evaluated as the logarithmic response sensitivities[34] of the half-rise of the induction time

$$S_i = \frac{\ln\dfrac{t'_{1/2,i}}{t_{1/2}}}{\ln f} \qquad (7)$$

where $t_{1/2}$ is the reaction time for the OH absorption to reach one-half of the maximum value, computed with a preliminary reaction mechanism; $t'_{1/2,i}$ is computed with the same mechanism but with the rate coefficient of the ith reaction multiplied by the factor f, assumed in these sensitivity tests to be equal 5 and 1/5. Most of the experimental mixtures were chosen to maximize the sensitivity to k_1. One mixture, A, was selected for a high sensitivity to k_2, the second most influential parameter in the H_2–O_2 system. The results of the sensitivity analysis are illustrated for three mixtures in Figure 4.

2. The strength of the OH absorption signal. The initial concentrations of H_2 and O_2 were selected to maintain sufficiently large signal-to-noise ratio (S/N). In most of the series, B–F, which employed a single absorption path through the shock tube, this ratio was kept above 100. In series A, having the lowest H_2 concentration, the signal was relatively weak and therefore a

(28) Schmidt, S. C.; Malte, P. C. *J. Quant. Spectrosc. Radiat. Transfer* **1976**, *16*, 963.
(29) Herzberg, G. *Molecular Spectra and Molecular Structure: I. Spectra of Diatomic Molecules*; Van Nostrand: Princeton, NJ, 1950; p 106.
(30) Lewis, G. N.; Randall, M. *Thermodynamics*; McGraw-Hill: New York, 1961; p 435.
(31) Smith, M. A. H.; Rinsland, C. P.; Fridovich, B.; Rao, K. N. In *Molecular Spectroscopy: Modern Research*; Rao, K. N., Ed.; Academic Press: New York, 1985; Vol. 3, p 111.
(32) Mitchell, A. C. G.; Zemansky, M. W. *Resonance Radiation and Excited Atoms*; Cambridge University Press: London, 1971.
(33) Rea, E. C., Jr.; Chang, A. Y.; Hanson, R. K. *J. Quant. Spectrosc. Radiat. Transfer* **1987**, *37*, 117.
(34) Frenklach, M. In *Combustion Chemistry*; Gradiner, W. C., Jr., Ed.; Springer-Verlag: New York, 1984; p 423.

TABLE I: Experimental Conditions and Results

T_5, K	P_5, atm	$C_5 \times 10^5$, mol cm^{-3}	$t_{1/4}$, μs	$t_{1/2}$, μs	$t_{3/4}$, μs	k_1,[b] cm^3 mol^{-1} s^{-1}	T_5, K	P_5, atm	$C_5 \times 10^5$, mol cm^{-3}	$t_{1/4}$, μs	$t_{1/2}$, μs	$t_{3/4}$, μs	k_1,[b] cm^3 mol^{-1} s^{-1}
Series A: 0.1% H_2–0.9% O_2–Ar													
1560[a]	2.05	1.60	218.4	243.0	259.5	1.02 (+12)	2166	2.76	1.55	54.5	60.5	65.5	2.27 (+12)
1674	2.19	1.60	172.0	187.6	200.3	1.03 (+12)	2189[a]	2.84	1.58	47.5	56.2	62.3	2.44 (+12)
1682	2.20	1.60	155.0	168.9	179.8	1.34 (+12)	2258	2.89	1.56	40.5	48.1	54.1	2.99 (+12)
1848	2.44	1.61	112.7	126.7	136.6	1.12 (+12)	2297	2.91	1.54	41.2	45.7	50.7	3.06 (+12)
1861	2.39	1.57	107.5	118.9	128.0	1.35 (+12)	2451	3.16	1.57	29.1	36.1	41.5	3.16 (+12)
1886	2.43	1.57	94.0	106.4	114.3	1.64 (+12)	2577	3.32	1.57	22.8	28.2	31.7	4.22 (+12)
2006	2.58	1.57	71.5	79.0	85.0	2.14 (+12)	2680[a]	3.41	1.55	19.7	22.8	26.3	5.93 (+12)
2103	2.70	1.56	59.2	65.8	71.5	2.32 (+12)	2691	3.43	1.54	16.3	20.2	23.6	9.62 (+12)
Series B: 0.5% H_2–1.0% O_2–Ar													
1396	1.87	1.63	182.8	197.2	209.9	5.10 (+11)	1939	2.48	1.56	41.2	45.9	50.0	1.52 (+12)
1397	1.87	1.63	156.2	172.2	185.5	6.50 (+11)	2034	2.64	1.58	31.9	36.2	39.1	1.84 (+12)
1414[a]	1.84	1.59	163.3	178.8	192.2	5.93 (+11)	2040	2.63	1.57	34.1	37.2	39.5	1.75 (+12)
1502	1.93	1.57	119.2	129.6	140.8	7.89 (+11)	2050	2.67	1.59	33.6	36.7	39.1	1.72 (+12)
1518	2.01	1.61	130.2	141.8	150.9	6.03 (+11)	2069	2.69	1.58	30.0	32.9	35.9	2.04 (+12)
1585	2.07	1.59	106.7	114.0	119.1	7.36 (+11)	2180	2.77	1.55	24.5	27.6	29.7	2.31 (+12)
1622	2.14	1.61	98.3	107.6	114.8	7.15 (+11)	2235	2.88	1.57	23.7	25.9	27.8	2.27 (+12)
1795	2.35	1.60	59.0	65.9	72.5	1.08 (+12)	2256	2.92	1.58	21.6	23.9	26.2	2.51 (+12)
1796	2.35	1.60	58.5	65.2	69.6	1.09 (+12)	2257[a]	2.84	1.53	22.3	24.4	26.4	2.54 (+12)
1811	2.31	1.56	57.5	64.1	70.6	1.14 (+12)	2258	2.90	1.56	19.6	22.8	25.0	2.79 (+12)
1859	2.34	1.54	55.4	59.5	62.8	1.18 (+12)							
Series C: 0.5% H_2–0.5% O_2–Ar													
1536[a]	2.01	1.60	175.5	191.8	207.5	7.41 (+11)	1806[a]	2.31	1.56	84.1	92.8	100.3	1.31 (+12)
1583	2.08	1.60	164.6	174.2	185.1	7.68 (+11)	1901	2.45	1.57	67.9	75.3	82.2	1.50 (+12)
1621	2.10	1.58	132.2	145.1	156.3	9.50 (+11)	1958	2.52	1.57	54.6	59.2	64.1	2.00 (+12)
1714	2.24	1.60	111.4	123.4	131.7	9.80 (+11)	2158	2.75	1.55	35.9	41.0	45.2	2.59 (+12)
1751	2.28	1.58	99.1	108.6	116.8	1.12 (+12)	2298[a]	2.94	1.56	30.3	33.3	36.3	2.88 (+12)
Series D: 2.0% H_2–1.0% O_2–Ar													
1336	1.77	1.61	169.5	184.4	197.3	3.58 (+11)	1694[a]	2.19	1.57	49.2	52.5	55.3	1.04 (+12)
1380	1.80	1.58	132.0	143.1	151.6	4.65 (+11)	1816	2.38	1.60	38.2	41.0	43.9	1.19 (+12)
1393[a]	1.85	1.62	131.1	142.3	150.8	4.44 (+11)	1887	2.43	1.57	27.0	30.4	32.9	1.67 (+12)
1413	1.81	1.56	105.6	115.7	122.3	5.88 (+11)	1984	2.58	1.58	21.0	23.0	24.8	2.15 (+12)
1454	1.95	1.63	119.0	125.6	131.6	4.63 (+11)	2022	1.76	1.05	34.0	37.1	40.0	1.83 (+12)
1475	1.93	1.59	93.7	100.8	106.0	6.11 (+11)	2142	2.82	1.60	17.6	19.5	21.4	2.16 (+12)
1489	1.29	1.06	132.5	140.5	148.3	6.53 (+11)	2198	2.86	1.58	13.6	15.5	17.1	2.87 (+12)
1543	1.99	1.58	80.2	85.4	91.0	6.86 (+11)	2269	1.97	1.06	20.9	23.2	25.4	2.58 (+12)
1582	2.03	1.56	66.6	71.3	75.0	8.28 (+11)	2341[a]	3.03	1.58	10.4	12.4	14.3	3.40 (+12)
1591	2.07	1.57	75.0	79.5	84.8	7.01 (+11)	2356	3.04	1.57	10.0	11.8	13.3	3.58 (+12)
Series E: 2.0% H_2–0.5% O_2–Ar													
1435[a]	1.92	1.63	190.5	206.3	221.7	4.94 (+11)	1915	2.47	1.57	47.3	52.5	56.4	1.54 (+12)
1482	1.92	1.58	139.5	156.6	164.6	6.67 (+11)	2022	2.60	1.57	36.6	40.8	43.6	1.89 (+12)
1571	2.04	1.58	117.6	128.3	138.7	7.57 (+11)	2029	2.62	1.57	38.7	44.1	48.1	1.70 (+12)
1581	2.12	1.63	130.7	142.6	153.3	6.37 (+11)	2077	2.64	1.55	30.7	35.0	38.1	2.21 (+12)
1667	2.20	1.61	99.8	106.6	114.6	8.29 (+11)	2195	2.80	1.55	25.6	29.9	31.7	2.39 (+12)
1716	2.24	1.59	78.7	87.9	95.3	1.00 (+12)	2296[a]	3.01	1.60	20.0	23.3	26.2	2.87 (+12)
1846[a]	2.39	1.58	56.7	62.6	68.2	1.33 (+12)	2352	3.02	1.56	15.7	18.4	21.0	3.81 (+12)
Series F: 20.0% H_2–5.0% O_2–Ar													
1047[a]	1.37	1.592	216.0	218.3	220.7	8.66 (+10)	1190	1.57	1.602	85.5	86.7	88.2	1.66 (+11)
1143	1.52	1.620	103.5	104.5	105.9	1.46 (+11)	1234[a]	1.64	1.619	60.7	62.8	63.7	2.13 (+11)

[a] Experimental conditions selected for optimization. [b] Numbers in parentheses are powers of 10.

triple-absorption path was used with S/N > 50. Series F, having the highest concentrations of H_2 and O_2, was designed to have strong absorption at low temperatures.

3. The influence of gas-dynamic phenomena on kinetic measurements and data analysis. Two steps were taken in this regard. First, to minimize the effects of the boundary-layer growth, the H_2 and O_2 concentrations and the experimental conditions were limited to those that produced induction times shorter than about 250 μs. The second gas-dynamic limitation was that constant-pressure and constant-density reaction geometries, the two limits of shock-initiated combustion,[35] produced the same computational results for the "normalized" OH profiles, thus indicating negligible effect of the temperature change on the data analysis.

4. Uncertainty in the time zero of the reaction. The onset of chemical reaction in the present work was determined by the schlieren peak created by the passage of the reflected-shock front through the laser beam. The estimated uncertainty of this measurement was about 1 μs. We, therefore, limited mixture compositions and experimental conditions to those resulting in induction times longer than at least 10 μs, and in most cases longer than 20 μs.

The combined instrumental uncertainties of induction time measurements in the present work were estimated to be about ±5%.

Data Analysis

As was mentioned earlier, the extraction of kinetic information from the experimental data collected in this study was performed by matching the initial part of the OH absorption profiles: from the onset of reaction till the maximum in the absorption signal.

(35) Frenklach, M.; Bornside, D. L. *Combust. Flame* **1984**, *56*, 1.
(36) Sutherland, J. W.; Michael, J. V.; Pirraglia, A. N.; Nesbitt, F. L.; Klemm, R. B. *Symp. (Int.) Combust., [Proc.]* **1988**, *21*, 929.
(37) Michael, J. V.; Sutherland, J. W. *J. Phys. Chem.* **1988**, *92*, 3853.
(38) Albers, E. A.; Hoyermann, K.; Wagner, H. Gg.; Wolfrum, J. *Symp. (Int.) Combust., [Proc.]* **1971**, *13*, 81.
(39) Kircher, C. C.; Sander, S. P. *J. Phys. Chem.* **1984**, *88*, 2082.

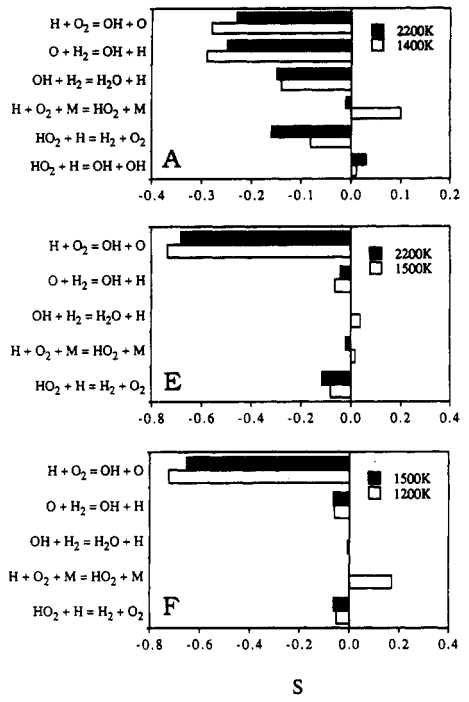

Figure 4. Logarithmic response sensitivity of $t_{1/2}$ with respect to active rate coefficients: (top) experimental conditions of series A, 0.1%H_2–0.9% O_2; (middle) series E, 2.0% H_2–0.5% O_2; and (bottom) series F, 20.0% H_2–5.0% O_2.

This was accomplished by fitting three representative points of the individual profiles, those corresponding to the attainment of 1/4, 1/2, and 3/4 of the maximum absorption. The rate coefficient determination was performed by matching the corresponding times, $t_{1/4}$, $t_{1/2}$, and $t_{3/4}$ (these are reported in Table I), with a chemical kinetic model.

The kinetic simulations were performed using a detailed reaction mechanism composed of 19 reactions and 8 chemical species. The reaction mechanism along with the rate coefficient expressions are given in Table II. All reactions were assumed to obey the principle of detailed balancing. The thermodynamic data for the calculations of the equilibrium constants were taken primarily from Burcat,[18] except for the heat of formation of HO_2 radical, which was taken from Hills and Howard,[40] who reported $\Delta_f H°_{298}$ = 3.0 kcal/mol. The kinetics of the H_2–O_2 system was computed by using an LSODE integrator:[41] series A–E with a constant-pressure code and series F with a constant-density code.

The analysis of the experimental data followed the technique of solution mapping.[42] The characteristic times $t_{1/4}$, $t_{1/2}$, and $t_{3/4}$ computed at 16 selected experimental conditions were expressed as algebraic functions of active (i.e., those which have measurable influence on the induction times) rate parameters by means of a prearranged set of computer experiments detailed below. The 16 sets of conditions were chosen, based upon initial screening of experimental data, as representative data points in each of the series; these sets are identified in Table I. The active rate parameters were determined by a screening sensitivity analysis. It

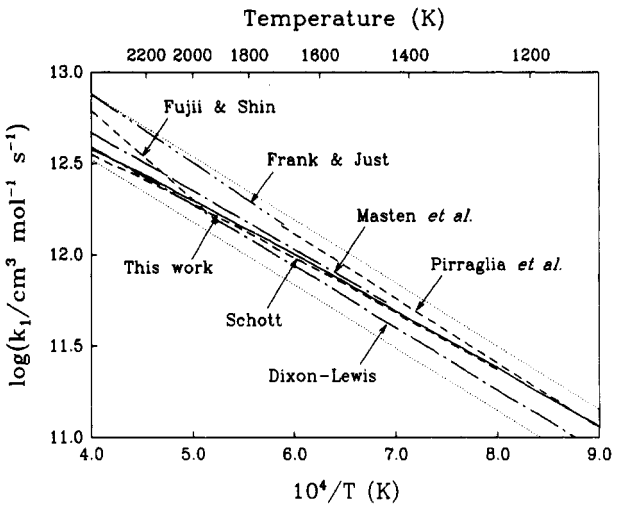

Figure 5. Arrhenius plot of experimentally determined rate coefficient expressions for reaction R1. The references are Dixon-Lewis,[8] Frank and Just,[9] Masten et al.,[43] Pirraglia et al.,[11] Schott.[6] The dotted lines enclose the variation range of k_1 assumed in the present work.

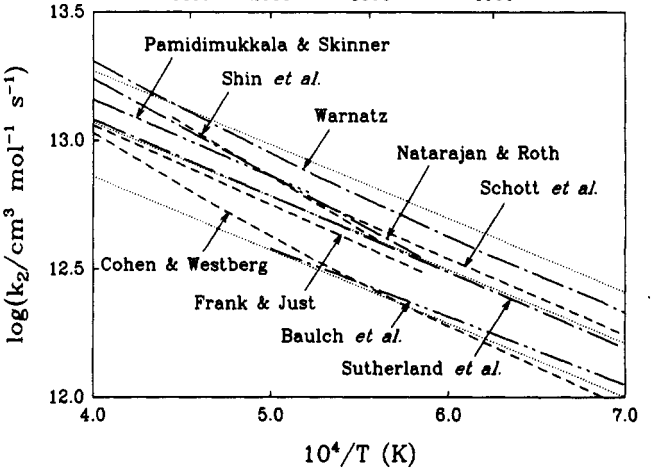

Figure 6. Arrhenius plot of suggested rate coefficient expressions for reaction R2. The references are Baulch et al.,[13] Cohen and Westberg,[14] Frank and Just,[9] Natarajan and Roth,[44] Pamidimukkala and Skinner,[45] Schott et al.,[46] Shin et al.,[47] Sutherland et al.,[36] Warnatz.[1] The dotted lines enclose the variation range of k_2 assumed in the present work.

was found that, besides being sensitive to k_1, the initial OH profile is also sensitive, though to a lesser degree, to rate coefficients of reactions

$$O + H_2 \rightarrow OH + H \quad (R2)$$

$$OH + H_2 \rightarrow H_2O + H \quad (R3)$$

$$H + O_2 + M \rightarrow HO_2 + M \quad (R8)$$

$$H_2 + O_2 + H \rightarrow HO_2 \quad (R-10)$$

The rate of reaction R8 had only limited influence on the computed induction times under the conditions of the present study and therefore k_8 was fixed at the value listed in Table II. The rate coefficient of reaction R–10, k_{-10}, was specified by using the principle of detailed balancing, and therefore k_{10} and $\Delta_f H°_{298}$-$(HO)_2$ were taken as active parameters for this reaction.

The computed characteristic times were then fitted with second-order polynomials

$$t_x^{calc} = \psi_x\{k_1, k_2, k_3, k_{-10}, \Delta_f H°_{298}(HO_2)\}, \quad x = \frac{1}{4}, \frac{1}{2}, \frac{3}{4} \quad (8)$$

using a factorial design. In developing these polynomials, the active

(40) Hills, A. J.; Howard, C. J. *J. Chem. Phys.* **1984**, *81*, 4458.
(41) Hindmarsh, A. C. "Towards a Systematic Collection of ODE Solvers". Presented at the 10th IMACS World Congress on System Simulation and Scientific Computation, Montreal, August 1982.
(42) Frenklach, M. In *Complex Chemical Reaction Systems, Mathematical Modelling and Simulation*; Warnatz, J., Jäger, W., Eds.; Springer-Verlag: Berlin, 1987; p 2.
(43) Masten, D. A.; Hanson, R. K.; Bowman, C. T. *J. Phys. Chem.* **1990**, *94*, 7119.
(44) Natarajan, K.; Roth, P. *Combust. Flame* **1987**, *70*, 267.
(45) Pamidimukkala, K. M.; Skinner, G. B. *J. Chem. Phys.* **1982**, *76*, 311.
(46) Schott, G. L.; Getzinger, R. W.; Seitz, W. A. *Int. J. Chem. Kinet.* **1974**, *6*, 921.
(47) Shin, K. S.; Fujii, N.; Gardiner, W. C., Jr. *Chem. Phys. Lett.* **1989**, *161*, 219.

TABLE II: Reaction Mechanism

no.	reaction	$\Delta H°_{2000K}$, kJ/mol	forward rate coefficient[b] A[c]	n	E	ref
1[a]	$H + O_2 \rightleftarrows OH + O$	65	1.59 (+17)	−0.927	70.6	this work
2[a]	$O + H_2 \rightleftarrows OH + H$	8	1.87 (+14)		57.0	36
3[a]	$OH + H_2 \rightarrow H_2O + H$	−62	6.32 (+13)		33.6	37
4	$OH + OH \cdot \cdot O + H_2O$	−70	2.10 (+08)	1.40	−1.7	14
5	$O + O + M \cdot \cdot O_2 + M$	−511	1.00 (+17)	−1.00		1
6	$H + H + M \cdot \cdot H_2 + M$	−454	6.40 (+17)	−1.00		1, 13
7	$H + OH + M \cdot \cdot H_2O + M$	−515	8.40 (+21)	−2.00		1, 13
8	$H + O_2 + M \cdot \cdot HO_2 + M$	−218	7.00 (+17)	−0.80		1
9	$HO_2 + H \cdot \cdot OH + OH$	−162	2.20 (+14)		5.9	8
10[a]	$HO_2 + H \cdot \cdot H_2 + O_2$	−236	2.50 (+13)		2.9	1, 13
11	$HO_2 + H \cdot \cdot H_2O + O$	−232	5.00 (+12)		5.9	8
12	$HO_2 + O \cdot \cdot O_2 + OH$	−227	2.00 (+13)			1
13	$HO_2 + OH \cdot \cdot H_2O + O_2$	−297	2.00 (+13)			1
14	$HO_2 + HO_2 \cdot \cdot H_2O_2 + O_2$	−156	1.06 (+11)		−7.1	38
15	$H_2O_2 + M \cdot \cdot OH + OH + M$	213	1.00 (+17)		190.4	1, 13
16	$H_2O_2 + H \cdot \cdot HO_2 + H_2$	−79	1.70 (+12)		15.8	1, 13
17	$H_2O_2 + H \cdot \cdot H_2O + OH$	−303	1.00 (+13)		15.0	1, 13
18	$H_2O_2 + O \cdot \cdot HO_2 + OH$	−71	2.80 (+13)		26.8	39
19	$H_2O_2 + OH \cdot \cdot H_2O + HO_2$	−141	7.00 (+12)		6.0	1

[a] Reaction whose rate coefficient was considered for optimization. [b] The forward rate coefficient $k = AT^n \exp(-E/RT)$; the units are cm³, K, kJ, mol, and s. The rate coefficients for the reverse direction were determined via equilibrium constants. [c] Numbers in parentheses are powers of 10.

TABLE III: Conditions and Results of Optimization[a]

run no.	k_1 A	n	E	k_2 A	n	E	k_3 A	n	E	k_{10} A	E	$\Delta_f H°_{298}(HO_2)$, kJ/mol	Φ_{min}	$\sigma_{\log k_1}$
1	5.36 (+15)	−0.507	66.06	4.30 (+08)	1.605	29.98	8.11 (+12)	0.009	0.70	2.22 (+13)	9.91	8.0	0.072	0.032
2	6.61 (+15)	−0.557	66.06	1.21 (+14)	0.000[b]	43.36	Michael and Sutherland[d]			Baulch et al.[e]		Hills and Howard[f]	0.096	0.034
3	2.32 (+16)	−0.715	67.03	2.52 (+14)	0.000[b]	54.93[c]	Michael and Sutherland[d]			Baulch et al.[e]		Hilss and Howard[f]	0.114	0.037
4	1.59 (+17)	−0.927	70.61	Sutherland et al.[g]			Michael and Sutherland[d]			Baulch et al.[e]		Hills and Howard[f]	0.201	0.048
5	1.71 (+17)	−0.935	70.67	Frank and Just[h]			Frank and Just[h]			Baulch et al.[e]		Hills and Howard[f]	0.168	0.044
6	1.71 (+17)	−0.949	70.62	Sutherland et al.[g]			Michael and Sutherland[d]			Baulch et al.[e]		Burcat[i]	0.157	0.043
7	3.96 (+15)	−0.434	68.28	Baulch et al.[e]			Baulch et al.[e]			Baulch et al.[e]		Hills and Howard[f]	0.720	0.092
8	1.21 (+14)	0.000[b]	66.06	3.56 (+13)	0.000[b]	31.59	Michael and Sutherland[d]			Baulch et al.[e]		Hills and Howard[f]	0.440	0.072
9	1.29 (+14)	0.000[b]	66.06	1.40 (+14)	0.000[b]	54.93[c]	Michael and Sutherland[d]			Baulch et al.[e]		Hills and Howard[f]	0.679	0.089
10	1.71 (+17)	−0.932	70.66	as in Masten et al.[j]			as in Masten et al.[j]			as in Masten et al.[j]		Hills and Howard[f]	0.181	0.046
11	1.71 (+17)	−0.950	69.60	Sutherland et al.[k]			Michael and Sutherland[l]			Baulch et al.[e]		Hills and Howard[f]	0.217	0.050

[a] The rate coefficients are in the form $k = AT^n e^{-E/RT}$ and the units are cm³, kJ, K, mol, s. Numbers in parentheses are powers of 10. [b] The variable is constrained to the value indicated. [c] The variable is constrained to the average activation energy of data displayed in Figure 6. [d] $k_3 = 6.32 \times 10^{13} e^{-33.63/RT}$; ref 37. [e] $k_2 = 1.8 \times 10^{10} T^{1.0} e^{-37.2/RT}$, $k_3 = 2.2 \times 10^{13} e^{-21.5/RT}$, $k_{10} = 2.5 \times 10^{13} e^{-2.9/RT}$; ref 13. [f] $\Delta_f H°_{298}(HO_2) = 12.6$ kJ/mol; ref 40. [g] $k_2 = 1.87 \times 10^{14} e^{-57.0/RT}$; ref 36. [h] $k_2 = 1.85 \times 10^{14} e^{-58.0/RT}$, $k_3 = 4.74 \times 10^{13} e^{-25.5/RT}$; ref 9. [i] $\Delta_f H°_{298}(HO_2) = 2.1$ kJ/mol; ref 18. [j] $k_2 = 5.06 \times 10^4 T^{2.67} e^{-26.3/RT}$ from ref 36, $k_3 = 1.17 \times 10^9 T^{1.3} e^{-15.2/RT}$ from ref 49, $k_{10} = 1.25 \times 10^{13}$ from ref 4. [k] $k_2 = 5.06 \times 10^4 T^{2.67} e^{-26.3/RT}$; ref 36. [l] $k_3 = 2.16 \times 10^8 T^{1.51} e^{-14.35/RT}$; ref 37.

variables were assumed to span over entire ranges of uncertainties, covering all the proposed values. This is illustrated in Figures 5 and 6, which show the assumed variation ranges of k_1 and k_2, respectively, by the dotted lines. Further details on polynomial functions (8), including the design matrix, explicit form of eq 8, and obtained coefficient values, are provided as supplementary material of this paper. (See Supplementary Material Available paragraph at the end of this article.)

The rate coefficients were determined by minimization of objective function

$$\Phi(\vartheta) = \sum_{r=1}^{16} \omega_r \sum_{i=1}^{3} \left(\frac{t_{i/4,r}^{expl} - \psi_{i/4,r}(\vartheta)}{t_{i/4,r}^{expl}} \right)^2 \qquad (9)$$

where ϑ is the vector of optimization variables and ω_r is the statistical weight assigned to the rth set of experimental conditions. The statistical weights were assumed to be unity for all the conditions except for those of series A. The experiments of the latter series had weaker absorption signals, and hence lower signal-to-noise ratios, and were carried out with the triple absorption path, resulting in larger uncertainty in the time zero determination due to widening of the schlieren peak. To take these larger uncertainties into account, statistical weights for this series of experiments were lowered to 0.5.

Results and Discussion

The optimization of objective function 9 was carried out using computer program ZXMWD of the International Mathematical & Statistical Libraries.[48] It was initially carried out in 12 variables: $\vartheta = \{A_1, n_1, E_1; A_2, n_2, E_2; A_3, n_3, E_3; A_{10}, E_{10}; \Delta_f H°_{298}(HO_2)\}$, where A_i, n_i, and E_i are the parameters of modified Arrhenius rate coefficient expression $AT^n e^{-E/RT}$ of reaction i. The unconstrained optimization resulted in physically unrealistic rate coefficients for secondary reactions. This indicated that the experimental data of the present study are insufficient to resolve the uncertainties for all the chosen optimization variables at once. Therefore, the optimization strategy adopted was to minimize the objective function imposing different constraints upon the variables.

The conditions and results for a selected number of optimization runs are presented in Table III. Run 1 in this table is the unconstrained optimization. All the other runs were carried out constraining the optimization variables in the manner indicated in the table. For instance, in run 2, the rate coefficients of reactions R3 and R10 and the heat of formation of HO_2 radical were fixed at some literature values and the optimization of (9) was carried out with respect to five variables: three parameters of the modified Arrhenius expression for k_1 and two of the Arrhenius expression for k_2. In run 3, the activation energy of k_2 was also fixed to an "average" of the data reported in Figure 6. Shown for each run in Table III is the value of objective function Φ attained at the respective minimum, Φ_{min}. The last column in Table III contains

(48) Rice, J. R. *Numerical Methods, Software, and Analysis: IMSC Reference Edition*; McGraw-Hill: New York, 1983.

(49) Dixon-Lewis, G.; Williams, D. J. In *Comprehensive Chemical Kinetics*; Bamford, C. H., Tipper, C. F. H., Eds.; Elsevier: Amsterdam, 1977; Vol. 17, Chapter 1.

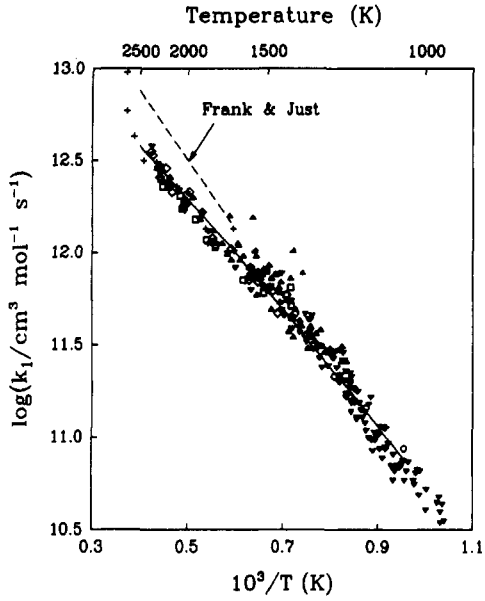

Figure 7. Arrhenius plot of rate data for reaction R1: (+) series A; (□) series B; (△) series C; (◇) series D; (▽) series E; (○) series F; (▲) experimental data of Pirraglia et al.[11] obtained with H_2O as the source of H atoms; (▼) experimental data of Pirraglia et al.[11] obtained with NH_3 as the source of H atoms; solid line, eq 11; dashed line, ref 9.

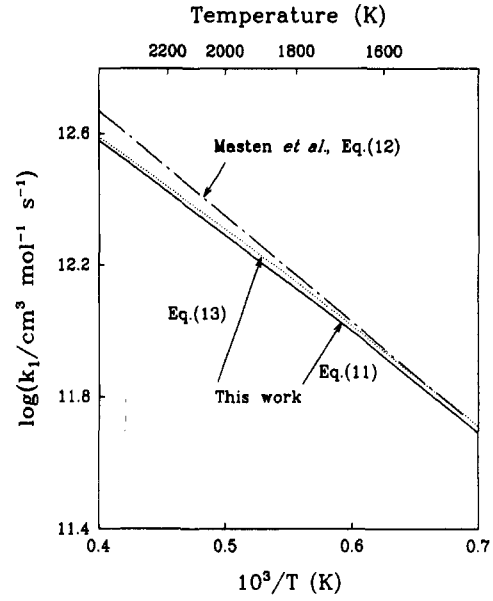

Figure 8. Arrhenius plot comparing results for k_1 obtained in this work with those of Masten et al.[43] (see text).

the value of one standard deviation for the logarithm of k_1, calculated as

$$\sigma_{\log k_1} = \frac{1}{2.3\langle S_1 \rangle}\left[\frac{\Phi_{\min}}{48 - \nu}\right]^{1/2} \qquad (10)$$

where $\langle S_1 \rangle$ is the average logarithmic response sensitivity of induction time with respect to k_1 (i.e., the average value of $\partial \ln t_v/\partial \ln k_1$), equal in our work to approximately 0.6; ν is the number of parameters determined; and 48 is the number of responses: three characteristic times for each of the 16 sets of experimental conditions employed in optimization.

The results of the performed optimization runs, constrained and unconstrained, all indicated that under no physically realistic conditions do the values of k_1 reach those reported by Frank and Just.[9] The obtained k_1 is increased with the decrease in k_2. Nonetheless, even for an extremely low k_2 (e.g., the one recommended by Baulch et al.,[13] see run 7 in Table III) the obtained k_1 is significantly lower than the expression of Frank and Just.[9] In most of the optimization runs, the resulting temperature-dependent expression for k_1 was found to be situated closer to the results of Schott.[6]

In light of low resolution of the present data toward all the active parameters, our present recommendation for k_1 is based on adopting the "best" literature values for the rest of the rate parameters. The result is (run 4 in Table III)

$$k_1 = 1.59 \times 10^{17} T^{-0.927} e^{-8493/T}, \quad \text{for } 1050 < T/\text{K} < 2700 \qquad (11)$$

in the units of $cm^3\ mol^{-1}\ s^{-1}$ with $\sigma_{\log k_1} = 0.05$ computed according to eq 10. To display graphically the final result (and to check the optimization procedure), the k_1 values were determined for individual experiments by fitting the $t_{1/2}$ data points under the same assumption as run 4 in Table III. The results of these calculations are reported in Table I and plotted in Figure 7. Also shown in Figure 7 are data of Pirraglia et al.[11] for determination of the rate coefficient of reaction R1. Although these authors[11] reported that a least-squares fit to their results agrees well with Frank and Just's rate expression for k_1, inspection of Figure 7 indicates that the rate data expressed as individual data points of Pirraglia et al.[11] and ours agree well with each other and actually show a continuous trend with a distinct bend around 1700 K. It can be also seen in the figure that the optimization result (11), shown as the solid line, goes through all the data points, indicating that the expression (11) can represent both sets of data. The obtained expression (11) is also in excellent agreement with the result of Schott,[6] $1.22 \times 10^{17} T^{-0.907} e^{-8369/T}$ for $1250 < T/\text{K} < 2500$; the difference between the two is less then 6%.

As this manuscript was prepared, we have learned about the new results of Masten et al.,[43] who employed a very similar OH diagnostic to measure the rate coefficient of reaction R1 in H_2–O_2–Ar mixtures behind incident and reflected shock waves. Their result

$$k_1^{\text{MHB}} = 9.33 \times 10^{13} e^{-7448/T}, \quad \text{for } 1450 < T/\text{K} < 3370 \qquad (12)$$

is slightly higher than ours (see Figure 8). Performing an optimization of (9) with the rate coefficients of secondary reactions used by Masten et al.[43] (see run 10 in Table III), we obtained the expression

$$k_1 = 1.71 \times 10^{17} T^{-0.932} e^{-8498/T} \qquad (13)$$

which differs from eq 11 by about 3%. This means that the difference between our results, eq 11, and those of Masten et al.,[43] eq 12, although still within the experimental uncertainties (e.g., at 2000 K expressions 11 and 12 differ by about 10%), cannot be explained entirely by the different choices of secondary parameters in the two works.

A close experimental consistency between our and Stanford[43] results can be used to address the following issue. The experiments of Masten et al.[43] were carried out behind both incident and reflected shock waves and indicated no upward bending in k_1 at high temperatures observed by Fujii and Shin[10] and exhibited by the two extreme experimental points in our series A (see Table I and Figure 7). We conclude therefore that at temperatures above 2600 K in our experimental system the chain branching of H_2–O_2 was influenced by impurities, which, taking into account the results of the blank tests with oxygen, are likely to be caused by degasing from the shock tube walls. It might be that the experiments of Fujii and Shin[10] were also influenced by similar impurities, and for the more dilute mixtures used in their study the effect appeared at lower temperatures.

Finally, we note that the main uncertainty in determination of the rate coefficient k_1, as well as in most other similar situations, are the systematic "errors" associated with the uncertainties in rate parameters of secondary reactions. The method of solution mapping allowed us to quantify these uncertainties in a rigorous mathematical manner, expressed by eqs 9 and 10. In fact, this representation specifies all the kinetic information extractable from the experimental data collected in the present study. To resolve the encountered uncertainty would require further experimental

measurements, such that the data collected increase the number of degrees of freedom of the objective function Φ.

Summary and Conclusions

OH radicals produced in shock-heated hydrogen-oxygen mixtures were monitored by state-selective laser absorption. The experimental conditions were chosen to maximize the sensitivity of the absorption signal to the rate coefficient of the title reaction, $H + O_2 \xrightarrow{k_1} OH + O$. Data analysis indicated, nonetheless, a significant influence of the rate parameters of the secondary reactions on the determination of k_1. Adopting the "best" literature values for these secondary parameters, our present recommendation for k_1, over the temperature range 1050-2700 K, is $1.59 \times 10^{17} T^{-0.927} e^{-8493/T}$ cm^3 mol^{-1} s^{-1} with one standard deviation of 0.05 for log k_1. This result is in good agreement with most recent experimental studies of this reaction, those of Schott,[6] Pirraglia et al.,[11] Masten et al.,[43] and the low-temperature results of Fujii and Shin,[10] but inconsistent with the expression of Frank and Just[9] and the high-temperature data of Fujii and Shin.[10]

Acknowledgment. The computations were performed using the facilities of the Penn State Center for Academic Computing. The laser facilities were purchased with NSF instrumentation grant no. CBT 85-14063. The work was supported by the Gas Research Institute, Contract No. 5086-260-1320.

Supplementary Material Available: Explicit form of eqs 8 and tables listing the design matrix and coefficient values (10 pages). Ordering information is given on any current masthead page.

Stochastic Effects in Propagation of Impulses: The Belousov-Zhabotinskii Reaction

M. Frankowicz,*,†

Laboratoire de Physique Théorique des Liquides, Université Pierre et Marie Curie, Paris, France

A. L. Kawczyński, and J. Górecki

Institute of Physical Chemistry, Polish Academy of Sciences, Warsaw, Poland *(Received: June 5, 1990; In Final Form: August 23, 1990)*

A randomly perturbed medium approach is used to study stochastic effects in a spatially distributed, excitable system close to the Hopf bifurcation. The Belousov-Zhabotinskii reaction has been chosen for model calculations. The appearance and properties of target patterns can be explained within the framework of the model discussed.

Introduction

Microscopic spatial inhomogeneities are present in any experiment. They may be caused by microscratches, dust particles, noise in inflow and outflow parameters, etc. These local inhomogeneities can influence chemical processes, and this influence is especially important in nonlinear systems close to bifurcations, leading to observable effects.

Microscopic imperfections are beyond any control, so it seems reasonable to adopt the concept of a randomly perturbed medium to model their influence on a system's evolution. This concept has been used successfully in continuum mechanics and radiophysics,[1] and we have recently applied it to simulations of random effects in the propagation of trigger waves in a chemical system.[2] We investigate in this paper an excitable chemical system in the vicinity of a Hopf bifurcation. The ferroin-catalyzed Belousov-Zhabotinskii (BZ) reaction has been chosen as the model.

It is well-known that the BZ reaction[3,4] as well as a few others[5,6] produces ring waves in the form of target patterns in a thin layer of reagent. These patterns appear in a range of initial concentrations of reagents which corresponds to oscillatory as well as excitable regimes (at least in the BZ reaction). The waves develop from regions (points) where the frequency of oscillations is higher than in the surrounding reagent. One explanation of target patterns is based on the assumption that heterogeneities (pacemakers) increase the local frequency of oscillations, giving rise to ring waves.[7-9] Another possible explanation uses the idea of homogeneous centers (leading centers).[10,11] Experiments seem to confirm the existence of both types of centers.[12] Additional arguments concerning the presence of a particular type of center come from statistical studies. Some results have been published for the oscillatory regimes,[13-15] whereas for the excitable regime, to our best knowledge, no results are known. The aim of this paper is to investigate pacemaker formation in an excitable medium.

The Model

The chemistry of the BZ reaction is usually described by the Field-Koros-Noyes (FKN) model[16] consisting of 11 reactions with 12 chemical species. This model can be simplified, still retaining the qualitative features of the complete FKN mechanism. A simplified two-variable model of the ferroin-catalyzed BZ reaction has been proposed recently by Rovinsky and Zhabotinskii.[17] It

† Permanent address: Department of Theoretical Chemistry, Faculty of Chemistry, Jagellonian Uniwersity, Kraków, Poland.

(1) Sobczyk, K. *Stochastic Waves*, PWN: Warsaw, 1982.
(2) Frankowicz, M.; Kawczyński, A. L. *J. Phys. Chem.* **1989**, *93*, 2755.
(3) Zaikin, A. N.; Zhabotinskii, A. M. *Nature* **1970**, *225*, 535.
(4) Zhabotinskii, A. M. *Concentration Autooscillations*; Moscow, 1974 (in Russian).
(5) Pehl, K. W.; Kunert, L.; Linde, H. *Nature* **1979**, *262*, 199.
(6) de Kepper, P.; Epstein, I. R.; Kustin, K.; Orban, M. *J. Phys. Chem.* **1982**, *88*, 170.
(7) Ortoleva, P.; Ross, J. *J. Chem. Phys.* **1974**, *60*, 5090.
(8) Winfree, A. *The Geometry of Biological Time*; Springer: New York, 1980.
(9) Tyson, J. J.; Fife, P. C. *J. Chem. Phys.* **1980**, *73*, 2224.
(10) Zaikin, A. N.; Kawczyński, A. L. *J. Non-Equilib. Thermodyn.* **1977**, *2*, 39.
(11) Kawczyński, A. L. *Pol. J. Chem.* **1986**, *60*, 223.
(12) Vidal, C.; Pagola, A. *J. Phys. Chem.* **1989**, *93*, 2711.
(13) Smoes, M. L. In *Dynamics of Synergetic Systems*; Haken, H., Ed.; Springer: Berlin, 1980.
(14) Walgraef, D.; Dewel, G.; Borckmans, P. *J. Chem. Phys.* **1983**, *78*, 3043.
(15) Vidal, C.; Pagola, A.; Bodet, J. M.; Hanusse, P.; Bastardie, E. *J. Phys.* **1986**, *47*, 1999.
(16) Field, R. J.; Koros, E.; Noyes, R. M. *J. Am. Chem. Soc.* **1972**, *94*, 8649.
(17) Rovinsky, A. B.; Zhabotinskii, A. M. *J. Phys. Chem.* **1984**, *88*, 6081.

0022-3654/91/2095-1265$02.50/0